Ore Geology Reviews 96 (2018) 247–261

Contents lists available at ScienceDirect

Ore Geology Reviews

journal homepage: www.elsevier.com/locate/oregeorev

Differentiation of ironstone types by using rare earth elements and yttrium geochemistry – A case study from the Bahariya region, Egypt

A.M. Afify[a,b,*], M.E. Sanz-Montero[a], J.P. Calvo[a]

[a] Department of Petrology and Geochemistry, Faculty of Geological Sciences, Complutense University, Madrid, C/ José Antonio Nováis, 2, 28040 Madrid, Spain
[b] Department of Geology, Faculty of Science, Benha University, 13518 Benha, Egypt

ARTICLE INFO

Keywords:
Geochemistry
Rare Earth Elements
Yttrium
Ironstone
Bahariya
Egypt

ABSTRACT

This paper deals with the geological and geochemical characterization of ironstone deposits encountered in two different sedimentary successions (upper Cretaceous and lower Cenozoic) in northern Bahariya, Egypt. The ironstones occur as uneconomic thin bands, lenses and concretionary beds in Cenomanian clastic rocks of the Bahariya Formation and as economic iron ore associated with Eocene carbonate depositional units. The ironstones contain similar iron-bearing minerals, mainly goethite and hematite, which display a variety of fabrics, i.e. concretionary, massive, stromatolitic-like, oolitic, pisolitic, reniform aggregates, boxwork, liesegang, geode-like and brecciated. The iron-rich minerals preferentially replaced and/or cemented the primary and diagenetic (mainly dolomite) carbonates. Preservation of fabrics, sedimentary structures and thickness of the precursor carbonates is conspicuous.

Whole-rock composition of the Cretaceous ironstones shows lower Fe_2O_3 and MnO contents and relative enrichment in detrital-derived elements, namely Al, Zr and Nb, when compared with the Eocene ironstones, the latter showing enrichment in Fe, Mn, Si, and Ba oxides as well as Cu, Zn, Ni and Sr trace elements. Total REE content in the Cretaceous ironstones ranges widely from 70 to 348 ppm whilst the Eocene ironstones show quite low content, mostly from 1.96 to 31 ppm. Post Archean Australian Shale (PAAS)-normalized patterns of the upper Cretaceous ironstones display flat REE patterns, with small positive Eu and Pr, slightly negative Y and Ce anomalies which are close to unity and intermediate Nd concentrations (between 10 and 100 ppm). In contrast, PAAS-normalized REE + Y patterns of the Eocene ironstones display LREE positive slope with enriched flat HREE trend as well as negative Ce anomaly, positive Y and Eu anomalies, and low Nd concentration (in general less than 10 ppm).

Geochemical data along with sedimentary features of the upper Cretaceous and Eocene ironstones in Bahariya point to different origins in the two ironstone types, the former having been originated diagenetically whereas the latter were constrained by hydrothermal fluids. A syngenetic marine origin is ruled out for any of the studied ironstones. Higher amount of detrital derived elements as well as higher REE concentration in the upper Cretaceous ironstones than in the Eocene ironstones suggest some contribution from the associated clastic sediments. The negative Ce anomaly determined in both types indicates anoxic iron-rich solution that passed to oxidized surface. The presence of positive Y and Eu anomalies in the Eocene ironstones suggests that iron precipitation was favoured by hydrothermal reducing conditions, when slightly acidic fluids reached oxidizing alkaline waters.

1. Introduction

Ferruginous chemical sediments, such as ironstone deposits and banded iron formations (BIFs) are widely used as archives of geochemical proxies (Bau et al., 2014; Hein et al., 2016). The origin of iron ore deposits has long been subject of discussion and controversies. Furthermore, many genetic models have been proposed, opening a wide field for contrasting hypotheses (James, 1966; Stanton, 1972; Siehl and Thein, 1989; Heikoop et al., 1996; Mücke, 2000; Mücke and Farshad, 2005; Sturesson et al., 2000; Kappler et al., 2005; El Aref et al., 2006a; Loope et al., 2011; Bekker et al., 2010, 2014; Salama et al., 2012, 2013; Baioumy et al., 2013, 2014; Rasmussen et al., 2014; Sun et al., 2015; and references therein). Ferromanganese minerals can be formed through three main genetic processes, i.e. hydrogenetic, hydrothermal and diagenetic, and/or a combination of these processes (Hein et al., 1997) through different temporal and spatial occurrences. Type of

* Corresponding author.
E-mail address: adel_geol@yahoo.com (A.M. Afify).

https://doi.org/10.1016/j.oregeorev.2018.04.019
Received 12 June 2017; Received in revised form 16 April 2018; Accepted 19 April 2018
Available online 21 April 2018

fluids from which ferromanganese minerals were precipitated, i.e., marine/seawater, porewater and/or hot fluids are eventually varied according to the formation process (Hein et al., 1997; Bau et al., 2014). Primary deposition with superimposed lateritic weathering and hydrothermal alteration due to heated groundwater has been suggested as a genetic model for ironstones (e.g., Salama et al., 2012, 2013, 2014). Hydrothermalism and volcanicity are considered the main factors in controlling the formation of ferromanganese ore deposits and their associated minerals (e.g. sulfates, quartz and clays) in various geotectonic settings (Kimberley, 1989, 1994; Sturesson et al., 2000; Hein et al., 2008). Heikoop et al. (1996) reported the formation of iron ooids in reef areas under the influence of venting of hydrothermal water associated with volcanic activity. Similarly, hydrothermal solutions produce iron ooids in areas where erosion of volcanic rocks locally causes enrichment of the elements needed for ooid formation (Sturesson et al., 1999). In addition, Kimberley (1989, 1994) documented precipitation of iron from exhalative fluids associated with active faults. Replacement of carbonates (Kimberley, 1979; Loope et al., 2011; Afify et al., 2015a), crystallization from precursor iron oxyhydroxide gels (Harder, 1989), mechanical accretion of chamositic clay particles (Bhattacharyya and Kakimoto, 1982; Van Houten and Purucker, 1984), mixed marine/hydrothermal precipitation (Baioumy et al., 2014) and/or precipitation in shallow marine or submarine environments (Young and Taylor, 1989; Helba et al., 2001; El Aref et al., 2006a,b; Salama et al., 2012, 2013, 2014, 2015) linked to sedimentary exhalative hydrothermal processes in tectonically active areas (Rivas-Sánchez et al., 2006; Hein et al., 2016) are reported as mechanisms of ironstone formation.

Variations in mineralogy, geochemistry (major, trace and rare earth elements and yttrium (REE + Y)) could help in discriminating the origin of the fluids leading to the formation of ferromanganese deposits. Normalized REE + Y distribution patterns of the iron and manganese deposits are considered good proxies for determining fluid compositions, the mineralogy of the precursor phases, the depositional environments and/or the physical and chemical conditions of mineralization (Bau and Möller, 1992; Bau, 1996; Bau et al., 1996,2014; Owen et al., 1999; Chen et al., 2006; Hein et al., 2016). Likewise, REE + Y have been used as geochemical signatures because of their coherent behavior during geochemical processes and because of their predictable fractionation (Hein et al., 2016).

On this basis, comparison of two iron-bearing rock types occurring in a same area but formed under different geological conditions and timing offers an opportunity to better understanding the origin of ironstone deposits. For this purpose, we studied two different ironstone types from the upper Cretaceous – lower Tertiary sedimentary succession in the northern part of the Bahariya Depression of Egypt (Fig. 1). One ironstone type is hosted in siliciclastic rocks of the Cenomanian Bahariya Formation whereas the other type is mainly associated with the Eocene carbonate units (Fig. 1). An integrated approach using sedimentology and paleoenvironmental analysis of the host rocks and the associated ironstones was previously achieved (El Aref et al., 1999, 2006a,b; Helba et al., 2001; Tanner and Khalifa, 2010; Salama et al., 2012, 2013, 2014, 2015; Afify et al., 2015a,b, 2016). This paper provides additional new insight on the genesis of the ironstones after detailed mineralogical and geochemical investigation with more concern on the rare earth elements and yttrium geochemistry.

2. Geology of the study area and ironstone sedimentary features

The Bahariya Depression is located near the central part of the Western Desert of Egypt (Fig. 1). The area is characterized topographically by a plateau of karstified Eocene carbonates surrounding the depression. The outcrop succession in the area comprises, from bottom to top, the lower Cenomanian Bahariya Formation, the upper Cenomanian El Heiz Formation, the Campanian El Hefhuf Formation, and the Maastrichtian Khoman Chalk Formation. The upper Cretaceous formations are unconformably overlain by the Eocene Naqb, Qazzun and El Hamra formations (Fig. 1) and the Oligocene Radwan Formation. Basaltic to doleritic dykes, sills, laccoliths and lava flows of Miocene age (El-Etr and Moustafa, 1978; Meneisy, 1990) occur in the northern part of the depression (Fig. 1). The Bahariya area was deformed by four tectonic phases during the early Mesozoic, late Cretaceous, post-middle Eocene and middle Miocene respectively (Sehim, 1993; Moustafa et al., 2003; Afify et al., 2016). Three of these structural phases affected the exposed rock units of Bahariya where the deep seated normal faults that resulted from the early Mesozoic deformation phase were reactivated in the late Cretaceous and post Eocene by oblique slip faults and en-echelon folds (Sehim, 1993; Moustafa et al., 2003; Afify et al., 2015b, 2016).

The studied ironstones occur either as thin bands, irregular beds and concretions hosted in siliciclastic deposits of the Bahariya Formation throughout the basin (Fig. 2) or as economic iron ore bodies associated with Eocene rock units in three mine areas that are closely related to two fault systems (Fig. 1). A summary of the main features, i.e. occurrences, grade, thickness, morphology and distribution, of both ironstone types is shown in Table 1.

The ironstones hosted in the Cenomanian Bahariya Formation occur in its lower and upper units, though they are absent in the middle unit which, unlike the others, do not contain carbonate rocks (Afify et al.,

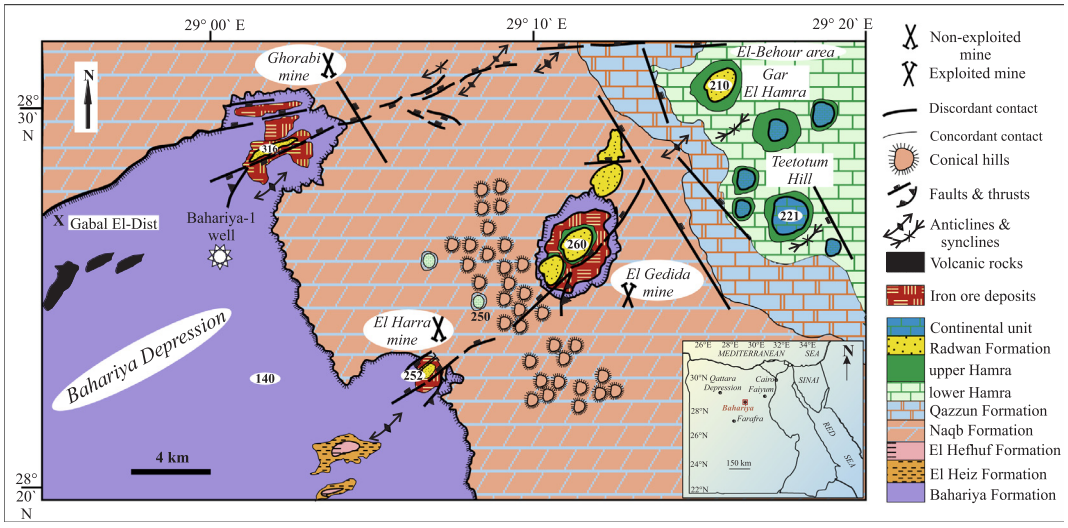

Fig. 1. Geological map of the northern Bahariya Depression (modified after Said and Issawi, 1964).

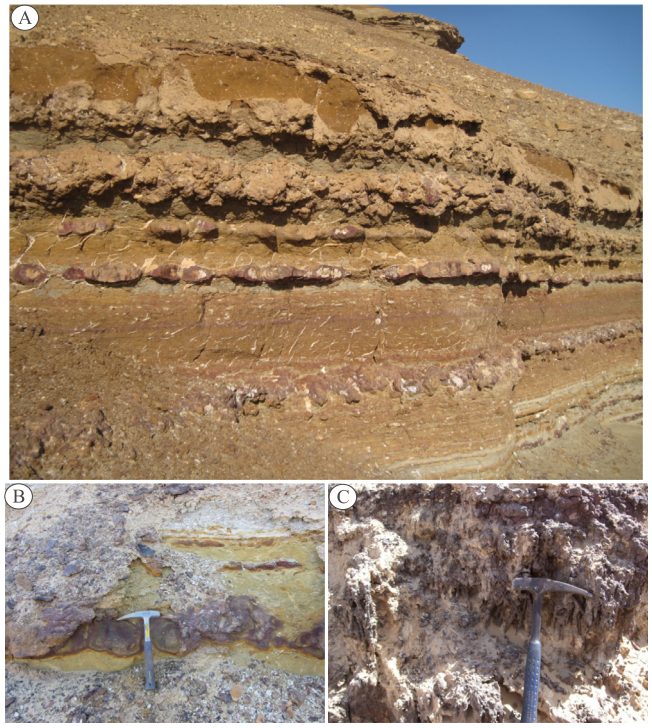

Fig. 2. Field photos showing variable sedimentary features of the upper Cretaceous ironstones within the Bahariya Formation, A. Thin ironstone crusts within the Cenomanian clastic rocks (height of photo = 2 m). B. Irregular concretionary ironstone bed. C. Rhizoliths of plant roots mainly replaced by iron oxyhydroxides.

2015a). On the basis of sedimentological and mineralogical analyses, sources of iron and formation of the upper Cretaceous ironstones were previously described by Mücke and Agthe (1988), El Aref et al. (1999), Mesaed (2006), Catuneanu et al. (2006), Tanner and Khalifa (2010) and Afify et al. (2015a). The latter revealed that they show selective replacement of iron-rich carbonates (Fe-dolomite, ankerite) that in turn replaced and/or cemented primary carbonate deposits, i.e. shell fragments, micrite, carbonate grains, calcrete and rhizoliths fabrics (Fig. 2). On the other hand, the Eocene ironstones occur as economic iron ore (Fig. 3) that are mainly concentrated in three mines; Ghorabi, El Harra and El Gedida areas (Fig. 1) (El Akkad and Issawi, 1963; Basta and Amer, 1969; El Sharkawi et al., 1984; El Aref et al., 1999; Dabous, 2002; El Aref et al., 2006a,b; Baioumy et al., 2013; Salama et al., 2012, 2014, and references therein). Comparison of these economic ironstone deposits with the Eocene carbonate rocks of the Naqb, Qazzun and lower Hamra formations revealed similar sequences, bedding structures, fossil contents and karstic features (Afify et al., 2015b, 2016). The Eocene ironstones are unconformably overlain by the upper Eocene glauconitic clay beds (upper Hamra unit; Afify et al., 2016) (Fig. 3). The ironstones hosted in the Eocene rocks show extensive replacement and cementation of both the dolostones of the Naqb Formation and the limestones of the Qazzun and the lower Hamra formations. Dating of the larger foraminifers from the youngest fossiliferous ironstone beds at El Gedida mine as early Bartonian gives indication that the replacement occurred during the Priabonian time, where sea level regression resulted in subaerial exposure that ultimately related to tectonic deformation of the area (Afify et al., 2016). The replacement was most probably coeval to the pisolitic ironstone formation on the topmost part of the ironstone succession at El Gedida area and before the deposition of the glauconitic overburden that was not affected by ironstone mineralization (Afify et al., 2016). The Eocene ironstones display a variety of fabrics, i.e., concretionary, massive, stromatolitic-like, oolitic, pisolitic, reniform aggregates, boxwork, geode-like and brecciated, that

Table 1
Summary and comparison of the main characteristics (sedimentary features, mineralogy, constraints and origin) of the upper Cretaceous and Eocene ironstones of the Bahariya region, Egypt.

Features	Upper cretaceous ironstones	Eocene ironstones
Occurrence and extension	Occurrence in the lower and upper units of the Cenomanian Bahariya Formation along the whole depression. Ironstone is absent in sandstones of the middle unit Ironstone occurs mainly in permeable carbonate rocks and sedimentary discontinuities	Local occurrence related to two major fault systems in the carbonate plateau of the northern Bahariya regionThe ironstones mainly replace carbonate rocks (limestone and dolostone) of the Eocene formations
Morphology	Thin crusts, irregular beds up to 1 m thick; also, as concretions up to 40 cm in diameter included in siliciclastic rocks	Large bedded and stratiform ironstones reaching up to 13 m in thickness at the Ghorabi and El Harra areas, up to 30 m at the El Gedida mine
Ore texture and structure	Massive, concretionary, brecciated, and leisegang-like rings and bandsMainly replacive textures including fossiliferous carbonate beds, calcrete fabrics (rhizoliths, etc.)	Preserved textures of skeletal and non-skeletal grains as well as structures of precursor carbonates, e.g., massive mud-supported, oolitic and stromatolitic fabrics. Pisolitic, box-work and concretionary fabrics are common
Iron-bearing minerals	Goethite, hematite, Fe-dolomite, ankerite and some siderite	Goethite, hematite, some jarosite (and pyrite?)
Associated non-iron minerals	Pyrolusite, romanechite, todorokite, barite, quartz	Quartz, pyrolusite, jacobsite, romanechite, psilomelane, todorokite, barite, alunite, apatite
Ore grade	Low-grade ironstone deposits in siliciclastic sediments	High-grade ironstone deposits, especially those of the El Gedida mine. The ore deposits of the Ghorabi and El Harra areas are of medium grade due to high quartz content
Mineral paragenesis	Subordinate iron oxyhydroxides formed during early diagenetic stages in paleosol horizons. Most iron oxyhydroxides precipitated in telogenetic stages after replacement of previously formed dolomite and ankerite phases	Ferromanganese minerals formed after or coeval to silicification of the Eocene carbonates. Sulfate minerals like barite formed after silica and Fe, Mn minerals through fractures and other types of pores
Ore controls	Mainly facies control. Selective replacement of carbonates associated with the siliciclastic rocks. Formation of the ironstones was favoured by uplift of the basin during the Late Cretaceous	Structurally-controlled. Ironstones formed along two major fault systems. This structure was related to the phase rifting and opening of the Gulf of Suez/Red Sea, which was accompanied by magmatic activity
Fluid migration	Enhanced by organic matter decomposition and hydrocarbon migration	Enhanced by tectonic activity (faulting as structure conduits) and magmatic activity
Timing	Turonian – Santonian uplift of the region	Upper Eocene (mostly Priabonian)
Source of iron	Dissolution of siderite, pyrite, Fe-dolomite of the Jurassic rocks (hydrocarbon-source rock) Other possible sources, i.e. iron-bearing minerals of the host rock	Hydrothermal iron-rich fluids migrated upwardly through the major fault system. These fluids mostly associated with a magmatic activity during upper Eocene that was before the main volcanic extrusive activity occurred during the Oligocene-Miocene in the Bahariya area

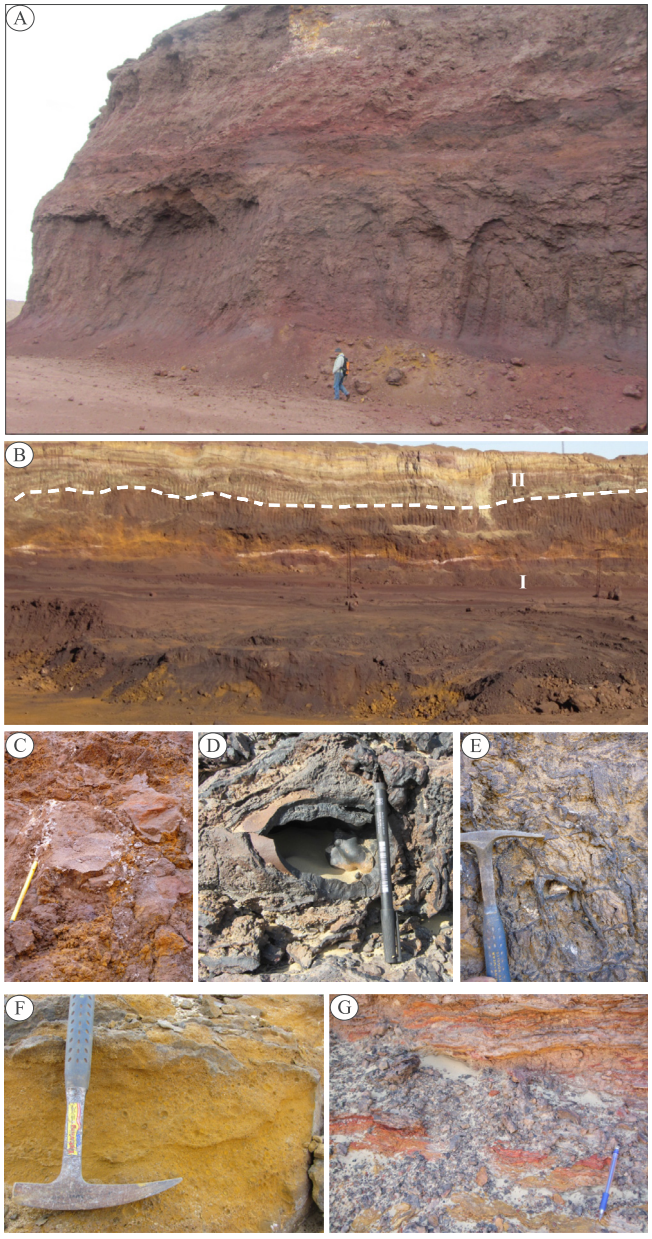

Fig. 3. Field photos showing the sedimentary features and fabrics of the Eocene ironstones at the mine areas, A-Outcrop view of big ore body of ironstones at the central part of the El Gedida mine area (See Fig. 1 for mine location). Outcrop view of the Eocene ironstone succession (I) unconformably overlain by upper Eocene glauconitic clays (II). C-Close-up view of brecciated goethitic ironstone with fractures-filling barite. D. Geodes of goethitic ironstone. E. Box-work structures of ironstones. F-Pisolitic ironstone. G-Stromatolitic-like ironstone.

preserve the textures and structures of the carbonate precursors (Afify et al., 2015b) (Fig. 3). The stromatolitic, ooidal and oncoidal ironstone fabrics were suggested to be of biogenic origin by Salama et al. (2013).

3. Analytical procedures

About 220 samples were collected from the host rocks and associated ironstones in both the Bahariya Formation and the Eocene rock units. Detailed petrographic, mineralogical and geochemical characterizations were carried out in the different ironstone samples. All of the hard samples were prepared for petrographic studies where 200 thin sections were done. Mineralogy of all collected samples was determined by XRD analyses using a Philips PW-1710 diffractometer and a Bruker D8 Advance diffractometer operating under monochromatic Cu Kα radiation (λ = 1.54060 Å) at 40kv and 30 mA. Fused discs from powder samples were prepared for energy dispersive X-ray fluorescence (ED-XRF) using a Bruker S2 RANGER X-ray fluorescence spectrometer with X-Flash Silicon Drift Detector to study major and trace elements geochemistry. Elemental analyses (in wt.%) and chemical composition determination of minerals were carried out on carbon-coated polished thin sections using a JEOL Superprobe JXA 8900-M wavelength dispersive electron microprobe analyzer (WDS-EMPA) equipped with four crystal spectrometers and beam diameter between 2 and 5 μm to minimize damage from the electron beam.

Rare earth elements and yttrium (REE + Y) geochemical analyses were carried out for 24 ironstone samples using inductively coupled plasma/mass spectrometry (ICP/MS) following an established analytical protocol and using international certified reference material for quality control. The analysis was achieved after digestion of 0.25 g of selected sample powder with 2 ml HNO_3 in a capped Teflon-lined vessel and left in an oven for two days and then evaporated to dryness. The sample was subsequently digested with 2 ml conc. HF in capped Teflon-vessel for one day in the oven. The solution was evaporated to dryness and then 1 ml of $HClO_4$ was added, and further diluted with 25 ml of 4% vol of HCl for analysis. The smoothness of a shale normalized REE + Y pattern is a simple, but reliable criterion to test the quality of a chemical analysis and to eliminate questionable data sets (Bau et al., 2014; Hein et al., 2016). Thus, REE + Y patterns (yttrium was inserted between Dy and Ho according to its ionic radius) are normalized to post-Archean Australian Shale (PAAS: McLennan, 1989) to detect resemblance in the different types of the studied ironstones. The behavior of yttrium is similar to that of the heavy rare earth elements, especially the holmium (Ho) (Jochum et al., 1986). Therefore, yttrium and holmium are coupled in many geochemical environments (Bau and Dulski, 1999). Discrimination between light-REE (LREE; La, Ce, Pr, and Nd), middle-REE (MREE; Eu, Gd, Tb, and Dy), and heavy-REE (HREE; Er, Tm, Yb, and Lu) is achieved when plotted together with Sm, Ho, and Y in spidergrams. Different discrimination diagrams are also plotted, e.g., Ce/Ce∗ anomaly against Nd concentration and Y_{SN}/Ho_{SN} values. Anomalies of Ce, Eu, La, Gd and Y were also calculated. The Eu, Ce, Pr, Gd and La anomalies, where shale normalized (SN), are calculated as:

$Eu/Eu* = 2Eu_{SN}/(Sm_{SN} + Gd_{SN})$, $Ce/Ce* = 2Ce_{SN}/(La_{SN} + Pr_{SN})$, $Pr/Pr* = 2Pr_{SN}/(Ce_{SN} + Nd_{SN})$, $La/La* = La_{SN}/(3Pr_{SN} - 2Nd_{SN})$, $Gd/Gd* = Gd_{SN}/(0.33Sm_{SN} + 0.67Tb_{SN})$ (Taylor and Mclennan, 1985; Bau and Dulski, 1996).

4. Results

4.1. Mineralogy and high resolution textural analyses

A combination of XRD, SEM/EDX, EMPA and petrographic analyses was applied to clarify the mineralogical history and composition of the deposits. The mineralogy of the two ironstone types is characterized by presence of goethite and hematite as the main iron oxyhydroxides, although the iron carbonates siderite, Fe-dolomite and ankerite are common in the ironstone bands, lenses and concretions of the Bahariya Formation (Table 1). Subordinate amount of pyrolusite, todorokite, psilomelane, iron-rich clays (glauconite and smectite) and barite are included in the paragenetic sequence of the upper Cretaceous ironstones as well (Afify et al., 2015a) (see Table 2 for chemical formulae of the minerals). The Eocene ironstones show a more complex mineral paragenesis comprising quartz and subordinate amount of jarosite, alunite, barite, pyrolusite, jacobsite, romanechite, psilomelane, todorokite, apatite, palygorskite and kaolinite (Table 1; see Table 2 for chemical formulae of the minerals) (Salama et al., 2012; Afify et al., 2015b).

The crystal morphologies, texture and distribution of the iron oxyhydroxides in the two ironstone types were modified depending on the

Table 2
Main iron and manganese-bearing minerals and their chemical formula (chemical composition of minerals after Deer et al., 1992).

Mineral class		Mineral	Chemical formula
Iron-bearing minerals	Oxides	Goethite	FeO·OH
		Hematite	Fe_2O_3
	Silicates	Glauconite	K Mg (Fe, Al) $(SiO_3)_6 \cdot 3H_2O$
		Nontronite	$Na_{0.3}Fe_2((SiAl)_4O_{10})(OH)_2 \cdot nH_2O$
	Sulfides	Pyrite	FeS_2
	Carbonates	Siderite	$FeCO_3$
		Ankerite	Ca)Mg, Fe)$(CO_3)_2$
		Fe-Dolomite	Ca (Mg, Fe) $(CO_3)_2$
		Fe-Calcite	(Ca, Fe) CO_3
Mn-bearing minerals	Mn-Oxyhydroxides	Pyrolusite	MnO_2
		Manganite	MnO·OH
		Rhodochrosite	$MnCO_3$
		Jacobsite	$Mn(Mg, Fe)_2O_4$
		Romanechite	$((Ba,H_2O)_2(Mn^{+4},Mn^{+3})_5O_{10})$
		Psilomelane	$Ba(Mn^{2+})(Mn^{4+})_8O_{16}(OH)_4$
		Manjiroite	$(Na, K)(Mn^{+4}, Mn^{+2})_8O_{16} \cdot n(H_2O)$
		Todorokite	$(Na, Ca, K, Ba, Sr)1\text{-}x(Mn, Mg, Al)_6O_{12} \cdot 3\text{-}4H_2O$
		Birnessite	$(Na_{0.3}Ca_{0.1}K_{0.1})(Mn^{4+},Mn^{3+})_2O_4 \cdot 1.5 \cdot H_2O$
		Cryptomelane	$K(Mn^{4+},Mn^{2+})_8O_{16}$

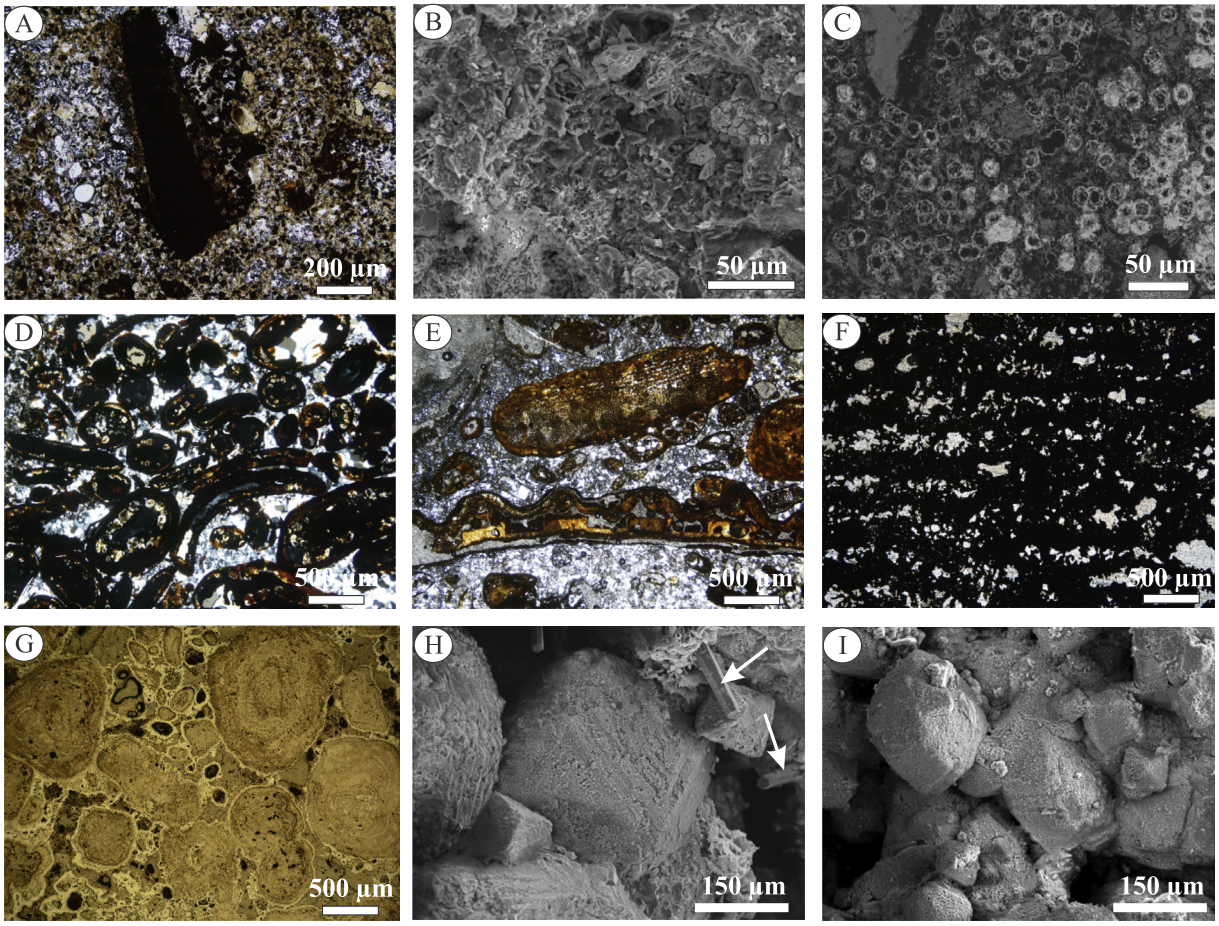

Fig. 4. Photomicrographs, scanning electron microscopic (SEM) and back-scattered electron (BSE) images of the iron-bearing minerals forming the upper Cretaceous (A–C) and Eocene (D–I) ironstones. A-Photomicrograph showing pseudomorphs of iron oxyhydroxides after dolomite/ankerite minerals still preserving their rhombic morphologies. B-SEM image of highly dissolved grey-colored dolomite crystals cemented by white-colored iron oxyhydroxides. C-BSE image of iron oxyhydroxides forming white-colored spherical crystals after rhombic dolomite/ankerite minerals. Note the grey colored carbonates that are still not replaced by iron. D–F-Photomicrographs of oolitic (D), fossiliferous (D, E) and stromatolitic-like (F) fabrics of ironstones preserving the skeletal and non-skeletal grains of their carbonatic precursors. G-Photomicrograph (in reflected light microscope) showing pisolitic fabrics of iron oxyhydroxides forming the ironstones at the topmost part of the Eocene succession. H, I-SEM images showing pseudomorphs of hematite mostly after pyrite cubic crystals, with few prismatic goethite (white arrows, H).

porosity, discontinuities, open-spaces and textures of the precursors. Using polarized-light and scanning electron microscopes, some iron oxyhydroxide cements exhibit primary open-space filling-textures (e.g., rosette-like, fibro-radiating, zoned-crystals). The iron-bearing minerals replace the carbonates of the Naqb, Qazzun and lower Hamra formations and preserve their main sedimentary features, i.e. lamination, oolitic, stromatolitic and fossiliferous fabrics (Afify et al., 2015a,b; Afify, 2016). Thus, it is possible to recognize easily the original skeletons of nummulites, alveolinids, mollusks, echinoids and ooids as well as the former textures of both the Cenomanian and the Eocene host rocks (Fig. 4). Likewise, dolomite of the Naqb Formation and/or ferroan dolomite/ankerite of the Bahariya Formation are present in the two ironstone types as relics, pseudomorphs, ghosts and/or crystalline rhombic aggregates (Fig. 4). Most of the carbonate textures and structures have been preserved in the two ironstone types hosted either in the Cenomanian clastic rocks (Fig. 4A–C) or in the Eocene carbonates (Fig. 4D–F). Pisolitic fabrics with irregular cortices of iron oxyhydroxides (Fig. 4G) are observed in the topmost part of El Gedida ironstone succession and the central part of Gabal Ghorabi (Salama et al., 2012, 2013, 2014). Chert, formed mainly of quartz is pervasive in some ironstone facies as both intergranular and intraparticle (Fig. 4D–F) cement and/or replacement. Cementation by quartz was preferential in the pores created by dissolution of carbonate bioclasts and found as pseudomorphs of dolomite crystals in the coarse-dolomitized and non-micritic parts (Afify et al., 2015b). Two genetic stages of quartz cementation/replacement were recorded; i.e., a first phase which is prior or contemporaneous with the iron oxyhydroxide precipitation and a second phase posterior to the main phase of iron oxyhydroxide formation (Afify et al., 2015b). Moreover, some hematite was observed to preserve scarce pyrite pseudomorphs at El Gedida area (Fig. 4H and I).

In summary, detailed petrographic analysis of the ironstones hosted in both the Cenomanian siliciclastic rocks and the Eocene carbonate deposits led us to conclude that they are mainly post-depositional showing selective replacement of carbonate minerals that preserve their original fabrics especially those of dolomite crystals.

4.2. Geochemistry

Geochemical data of the studied ironstone samples are presented in Appendices A, B, C and D (supplementary materials) and plotted in Figs. 5–11. These data represent the study of major oxides, trace and rare earth elements of the two ironstone types.

4.2.1. Major and trace elements geochemistry

The whole-rock composition of the upper Cretaceous ironstones shows high Fe_2O_3 content (≤73 wt%), and very low MnO content (≤2 wt%) (Appendix A; Fig. 5). In the carbonate-rich ironstone samples, CaO and MgO contents reach up to 12% and 8.5% respectively. The studied samples show relative enrichment in elements indicative of terrigenous input, i.e. Al_2O_3 (up to 7.89 wt%), SiO_2 (up to 21.8 wt%) and Na_2O (up to 7.8 wt%), which reach up even higher content in the clay-rich ironstone crusts (Appendix A, supplementary materials).

When compared with the upper Cretaceous ironstones, the whole-rock compositions of the Eocene ironstones are characterized by higher Fe_2O_3 (≤99.0 wt%) and MnO (up to 8.0 wt%) contents (Appendix B, supplementary materials). The CaO and MgO contents in these rocks are considerably lower than in the upper Cretaceous ironstones. The SiO_2 content increases in the more porous and fossiliferous facies reaching up to 75.6 wt% where the quartz mineral dominates (Appendix B; Fig. 6). The Eocene ironstones show very low Al_2O_3, Na_2O and K_2O content. The phosphorous content (P_2O_5) in the two ironstone types is very low and mostly below detection limit or less than 0.5 wt% (Appendices A, B, supplementary materials).

Trace element composition of the Eocene ironstones shows higher content in Zn (≤1138 ppm), Ni (≤719 ppm) and Sr (≤686 ppm) than that determined in the upper Cretaceous ironstone (112 ppm, 489 ppm and 339 ppm maximum values, respectively) (Appendices A, B; supplementary materials). Likewise, the Eocene ironstones show lower content in elements indicative of detrital input, such as Zr (≤78 ppm) and Nb (≤17 ppm) when compared with the upper Cretaceous ironstones: Zr (≤1065 ppm) and Nb (≤26 ppm).

Using electron microprobe (EMPA), slight geochemical differences arise when the iron-bearing minerals of the two ironstone types are considered separately. In the upper Cretaceous ironstones, the iron-bearing minerals show the following average content: FeO ≤ 78.0 wt%, MnO ≤ 2.2 wt%, MgO ≤ 4.8 wt%, CaO ≤ 2.8 wt%, SiO_2 ≤ 4.0 wt%, Al_2O_3 ≤ 2.0 wt% and P_2O_5 ≤ 0.6 wt% (Appendix C; Fig. 7). In contrast, in the iron-bearing minerals of the Eocene ironstones show higher content of FeO ≤ 83.0 wt%, MnO ≤ 8.3 wt% and BaO ≤ 10.0 wt% (Appendix D; Fig. 8). Moreover, the ferromanganese minerals of the Eocene ironstones are enriched in Ba and Mn but with very low Al and K (Appendix D; Fig. 8).

4.2.2. Rare earth elements and yttrium geochemistry

Data of rare earth elements and yttrium from both the Cretaceous and the Eocene ironstones are shown in Appendices A and B (supplementary materials) and plotted in Figs. 9–11. All selected samples for REE analyses are those with very low or without apatite or any other phosphate minerals where the P_2O_5 content not exceeds 0.5 wt% except three samples that reach up to 0.7 wt% (Appendices A, B; supplementary materials). Total REE content in the upper Cretaceous ironstones shows a wide range from 70 ppm to 348 ppm (Appendix A). In contrast, the Eocene ironstones show very low REE content, ranging from 1.96 ppm to 31 ppm, except for three samples showing 48, 60, 89 ppm (Appendix B). The silicified Eocene ironstones are depleted in REE showing a range from 1.96 to 6.85 ppm. In both rock types, light rare earth element (LREE) contents are higher than those of the heavy rare earth elements (HREE).

Rare earth elements and yttrium (REE + Y) geochemical data are normalized to Post Archean Australian Shale (PAAS; McLennan, 1989) (Figs. 9 and 10). The PAAS-normalized REE + Y spidergrams of the upper Cretaceous ironstones display similar flat REE patterns, with slight positive Eu, Pr and slight negative Ce anomalies which are close to unity (Appendix A; Fig. 9). PAAS-normalized REE + Y data for the Eocene ironstones display an initial drop from La to Ce followed by LREE positive slope with rise from the Ce minimum to the Eu maximum and with slight decrease towards a Lu minimum and enriched flat HREE trend (Fig. 10). When inserted between Dy and Ho, yttrium (Y) shows a very weak negative anomaly, which approaches the unity in the upper Cretaceous ironstones (Fig. 9). The REE + Y spidergrams from the Eocene ironstones show a more pronounced positive Y anomaly, but similar Ce and Eu anomalies than those determined in the upper Cretaceous ironstones (Figs. 9 and 10).

Following Bau et al. (2014)'s results, discrimination diagrams of Ce/Ce∗ vs. Nd concentration and Ce/Ce∗ vs. Y_{SN}/Ho_{SN} (SN: shale normalized) were used to distinguish between the different ironstone types. Using the same diagrams of Bau et al. (2014), the ironstones show negative to no Ce anomaly (Fig. 11). The upper Cretaceous ironstones show enrichment in Nd concentrations and fall in the 10–100 ppm range with positive correlation between Nd concentration and Ce/Ce∗ ratio (Fig. 11A). In contrast, the Eocene ironstones are characterized by low Nd concentrations ranging between 0.39 and 8.2 (less than 10 ppm) (Fig. 11A).

Regarding the representation of Ce anomaly vs. Y_{SN}/Ho_{SN} ratio (Fig. 11B), the upper Cretaceous ironstone samples show negative Y_{SN} values close to unity ($Y_{SN}/Ho_{SN} \leq 1$) whereas, the Eocene ironstones show positive Y_{SN} values ($Y_{SN}/Ho_{SN} \geq 1$), especially for the manganiferous and silicified, oolitic ironstones.

5. Discussion

The mineralogical and geochemical study of the two ironstone

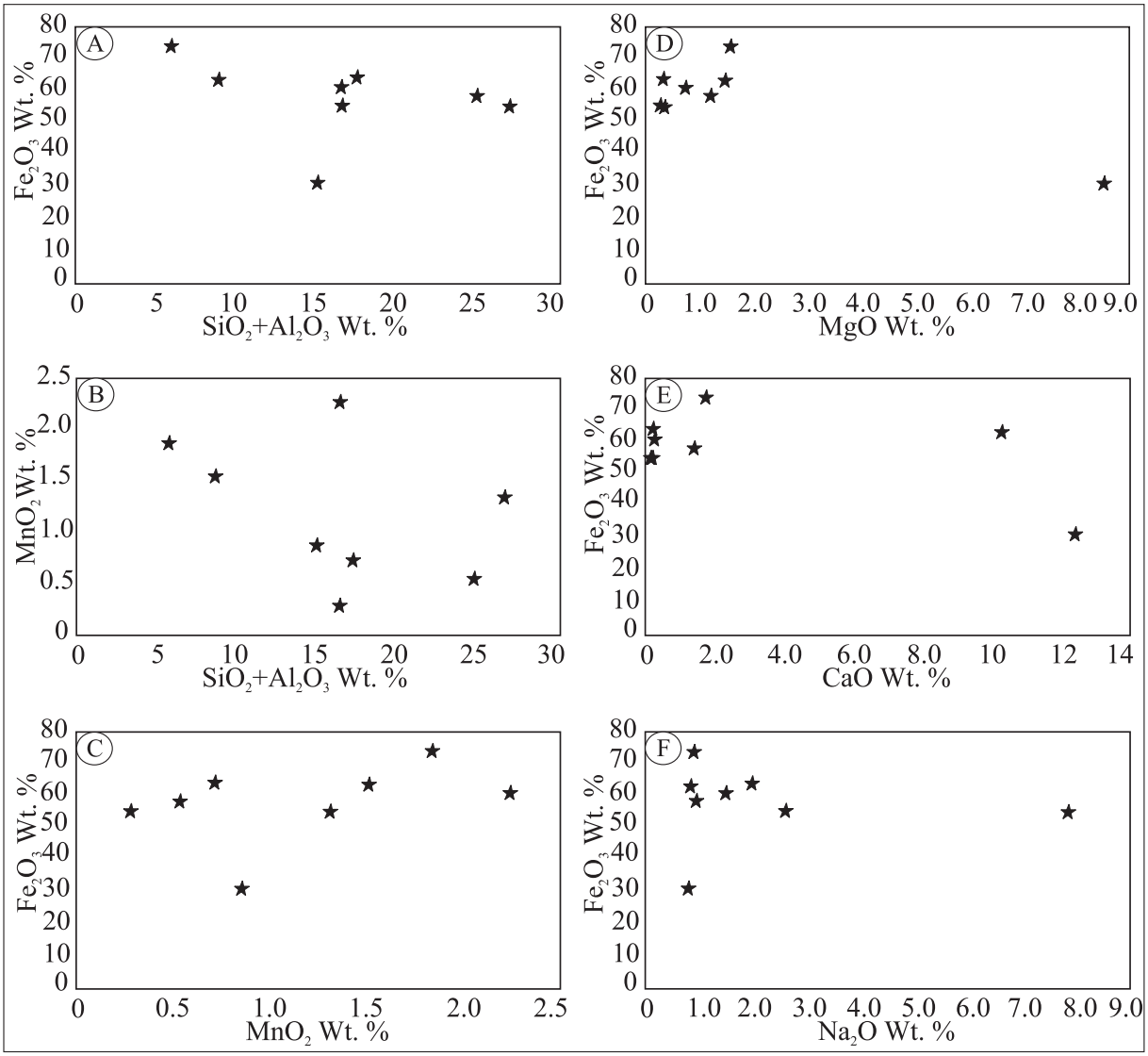

Fig. 5. Binary diagrams showing the bivariate relationships of Fe_2O_3 vs. $SiO_2 + Al_2O_3$ (A), MnO_2 vs. $SiO_2 + Al_2O_3$ (B) and Fe_2O_3 vs. MnO_2 (C), MgO (D), CaO (E), and vs. Na_2O (F) in the ironstones of the Bahariya formation. The values were determined by X-ray fluorescence.

types, which significantly occur in the same stratigraphic succession, not only provides useful signatures for discriminating and better understanding processes of ironstone formation but also allows to conclude that epigenetic hydrothermalism does not overprint the rare earth element and yttrium content of previously formed ironstones.

A variety of formation models and iron sources were proposed for the two ironstone types occurring in the Bahariya region. With regard to the upper Cretaceous ironstones, transformation of ilmenite detrital grains into rutile (Mücke and Agthe, 1988), pedogenesis (El Aref et al., 1999), the alteration and oxidization of glauconite (Mesaed, 2006; Catuneanu et al., 2006) and/or due to ground water activity, either during early diagenesis (Tanner and Khalifa, 2010) or during late diagenesis (telogenesis) (Afify et al., 2015a), were interpreted as a possible source of iron through laterization or diagenetic processes. Likewise, different genetic mechanisms were proposed for the upper Eocene ironstones; i.e., epigenetic, syngenetic-supergenetic, hydrothermal, lateritic, primary marine and/or mixed hydrogenous-hydrothermal origin (El Akkad and Issawi, 1963; Basta and Amer, 1969; El Aref and Lotfy, 1985; El Aref et al., 1999; Helba et al., 2001; Dabous, 2002; El Aref et al., 2006a,b; Salama et al., 2012, 2013, 2014; Baioumy et al., 2013, 2014 and references herein). The source of iron for these Cenozoic ironstone deposits varies according to the previously described genetic mechanisms. Thus, the underlying Bahariya Formation or the Nubia aquifer (Dabous, 2002; Salama et al., 2012, 2013, 2014), sea water precipitation to hydrothermal exhalites, and/or the surrounding Naqb Formation (Baioumy et al., 2013, 2014), iron leached from the overlying upper Eocene-lower Oligocene glauconitic clays (El Sharkawi et al., 1984; Dabous, 2002) are eventual sources of iron for the Eocene deposits.

Based on recent investigations by Afify et al. (2015a) and Afify et al. (2016), two contrasting genetic models, i.e. diagenetically-formed versus hydrothermal, are proposed, respectively, for the upper Cretaceous and the Eocene ironstones occurring in the Bahariya Depression (Fig. 12). The ironstone bands, lenses and concretions of the Cenomanian Bahariya Formation formed by replacement and/or cementation of dolomite and ankerite related to the migration of reducing iron-rich fluids through discontinuities and permeable facies at a basinal scale (Afify et al., 2015a). Thermal maturity after burial of the siliciclastics of the Bahariya Formation during the late Cretaceous (Metwalli and Pigott, 2005) probably accounted for the decomposition of organic matter and further hydrocarbon migration to the Bahariya Depression, which created reducing conditions favorable to bitumen formation and mobilization of iron-rich fluids (Afify et al., 2015a) in the region via groundwater with CH_4 or other hydrocarbons as reducing agents (Parry

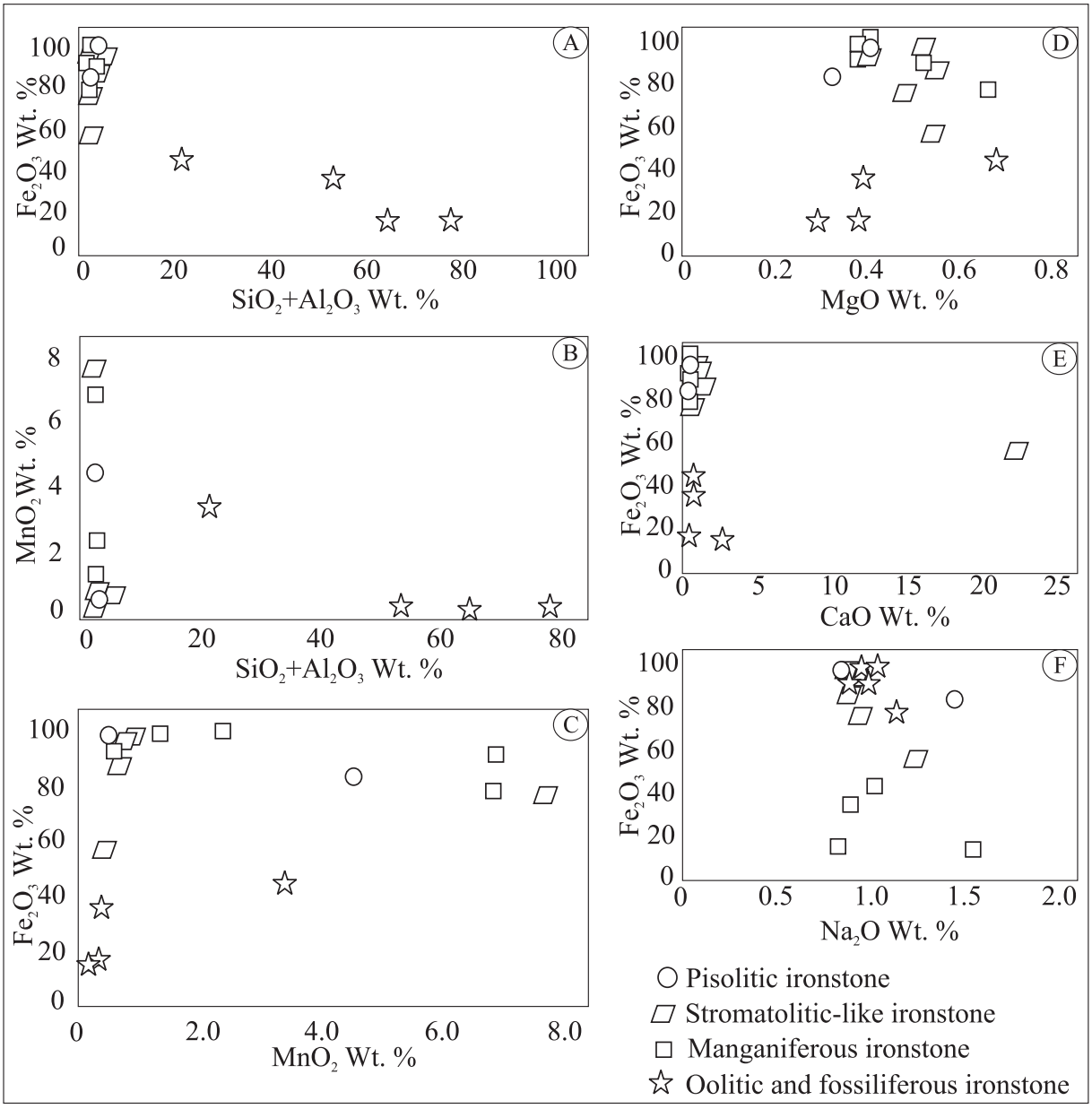

Fig. 6. Binary diagrams showing the bivariate relationships of Fe_2O_3 vs. $SiO_2 + Al_2O_3$ (A), MnO_2 vs. $SiO_2 + Al_2O_3$ (B) and Fe_2O_3 vs. MnO_2 (C), MgO (D), CaO (E), and vs. Na_2O (F) in the different Eocene ironstone types (manganiferous ironstone, oolitic and fossiliferous ironstone, stromatolitic-like ironstone and pisolitic ironstone) determined by XRF analysis.

et al., 2009; Parry, 2011) and/or organic acids (Chan et al., 2000). The iron-sourcing minerals could belong to the iron-bearing minerals associated with the Cenomanian Bahariya Formation or most likely the siderite, Fe-dolomite and pyrite of the underlying Jurassic Khatatba Formation which is a hydrocarbon-source rock in the north-Western Desert (Rossi et al., 2001, 2002). The Khatatba Formation is also present in the northern Bahariya Depression as confirmed by Bahariya 1 well in northern Bahariya Depression drilled by Devon Energy Egypt Companies (Moustafa et al., 2003).

In contrast, source of iron for the Eocene ironstones was mostly related to deep-seated hydrothermal iron-rich solutions that moved through major faults (Afify et al., 2015b). The latter postulated that these fluids were prior to the volcanic eruptions, which occurred in vicinity of the mine areas during Oligocene-Miocene (Meneisy, 1990). The replacement of the Eocene carbonate rock units (Naqb, Qazzun and lower Hamra formations) by iron minerals took place after Bartonian, most probably during the Priabonian (Afify et al., 2016). This dating is also consistent with the late Eocene – early Oligocene remagnetization event occurred in the Cenomanian rocks (Odah, 2004). The Eocene ironstone deposits were related to structural traps where hydrothermal reducing iron-rich fluids migrated through major fault systems (Fig. 1). In this setting, the reduced iron-rich fluids mixed with meteoric water in phreatic zones and a subsequent vadose phase involving preferential corrosion of carbonate host rocks by acid reducing fluids and subsequent oxidation of ferromanganese minerals under aerobic conditions.

The two differentiated models are supported by both mineralogical and geochemical evidence. Variations in mineralogy, major oxides and trace elements geochemistry as well as normalized REE distribution patterns of ironstones can be used to interpret the nature and origin of the forming fluids, the composition of the precursor mineral and/or the physical and chemical conditions in which mineralization processes took place (Sturesson et al., 2000; Mücke and Farshad, 2005; Bau et al., 2014; Hein et al., 2016).

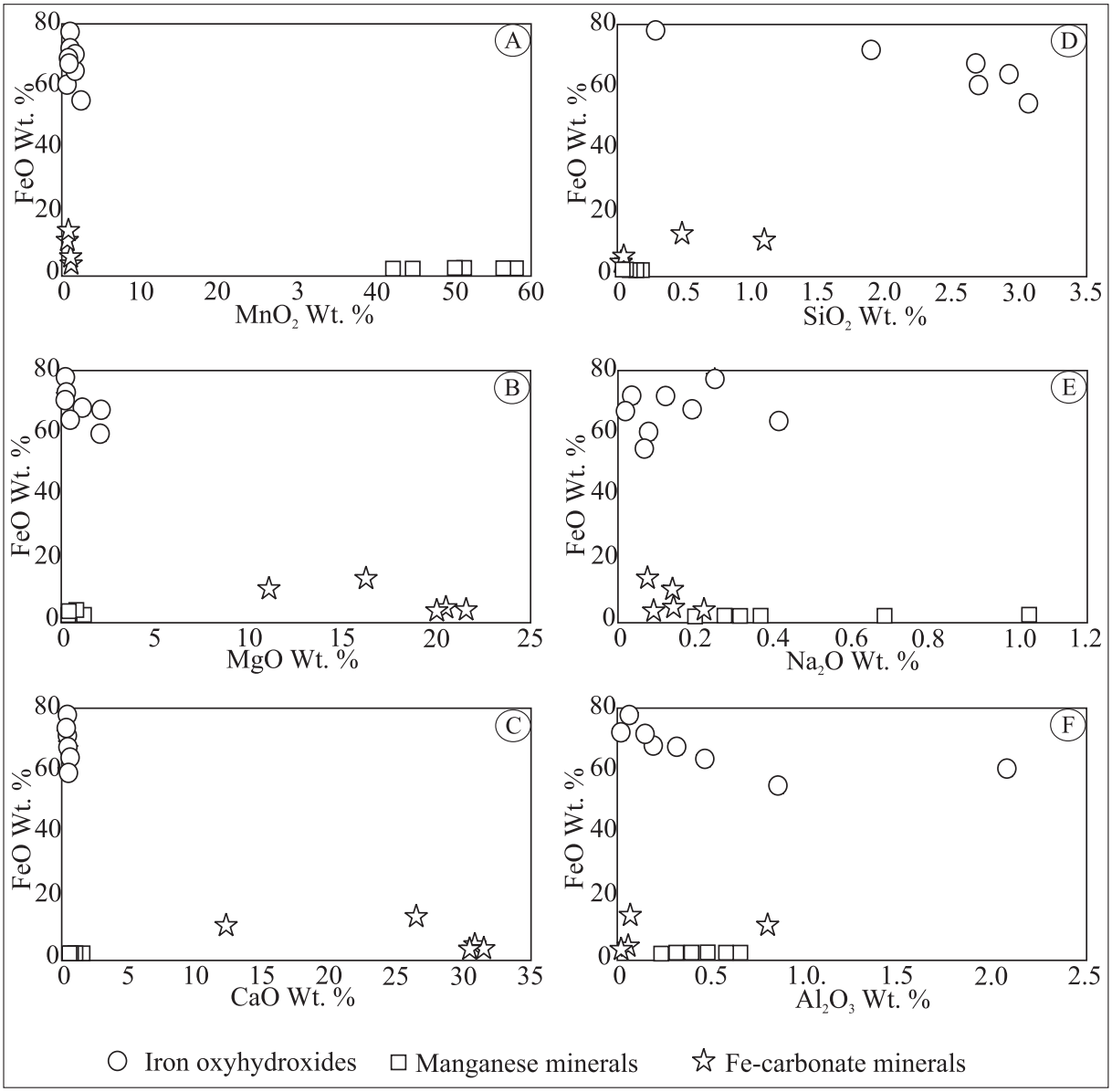

Fig. 7. Discrimination diagrams showing correlation between major oxides (FeO vs. MnO_2 (A), MgO (B), CaO (C), SiO_2 (D), Na_2O (E), and vs. Al_2O_3 (F)) in the three main minerals forming the upper Cretaceous ironstone crusts; values were determined by using electron microprobe analysis.

5.1. Evidence from major and trace elements

Altogether, geochemical insight and petrography reflect replacement of the primary and/or diagenetic carbonates by iron-bearing minerals, i.e., content of MgO and CaO which reaches up to (Appendices A, B) is coincident with the occurrence of carbonate relics and/or pseudomorphs supported by the petrographic evidence (Fig. 4) (Afify et al., 2015a,b). Relatively high MgO and CaO contents in the upper Cretaceous ironstones (Appendices A, C) are indicative of partial replacement of dolomite and ankerite by iron oxyhydroxides during telogenetic stages (Afify et al., 2015a). Regarding the Eocene ironstones (Appendices B, D), lower CaO and MgO contents than in the Cretaceous deposits suggest that replacement by Fe- and Mn-bearing minerals as well as cementation by quartz were actually important in the Eocene carbonates.

High trace element content of zirconium which reaches up to 1065 ppm recorded in bulk chemical analyses of the upper Cretaceous ironstone crusts (Appendix A) is mostly attributed to terrigenous derivation and/or large presence of clay minerals in the siliciclastic deposits, which is consistent with a relatively high content in detrital-derived major elements, i.e. Al_2O_3, SiO_2 and Na_2O. These values are in general higher than those determined in the Eocene ironstones. In the latter deposits, iron and manganese oxides and silica are higher than those of the upper Cretaceous counterparts, along with a considerably higher content of Ba, Cu, Zn, Ni and Sr trace elements, suggests that formation of the Eocene ironstones was enhanced mostly by hydrothermal input (Bekker et al., 2010; Baioumy et al., 2014; Hein et al., 2016) or by accumulation in a marine setting after weathering of older rocks (Salama et al., 2012). The elemental analyses of iron-bearing minerals for both ironstone types (Appendices C, D) reveal depletion in Al, Si, Na, K and Zn oxides, especially in the Eocene ironstones, which supports the exclusion of marine and/or terrigenous sources for these minerals (Nicholson, 1992; Hein et al., 2008; Bekker et al., 2010).

5.2. Discrimination of ironstone types and interpretation based on REE and Y content

Rare earth elements are especially useful in interpreting the origin

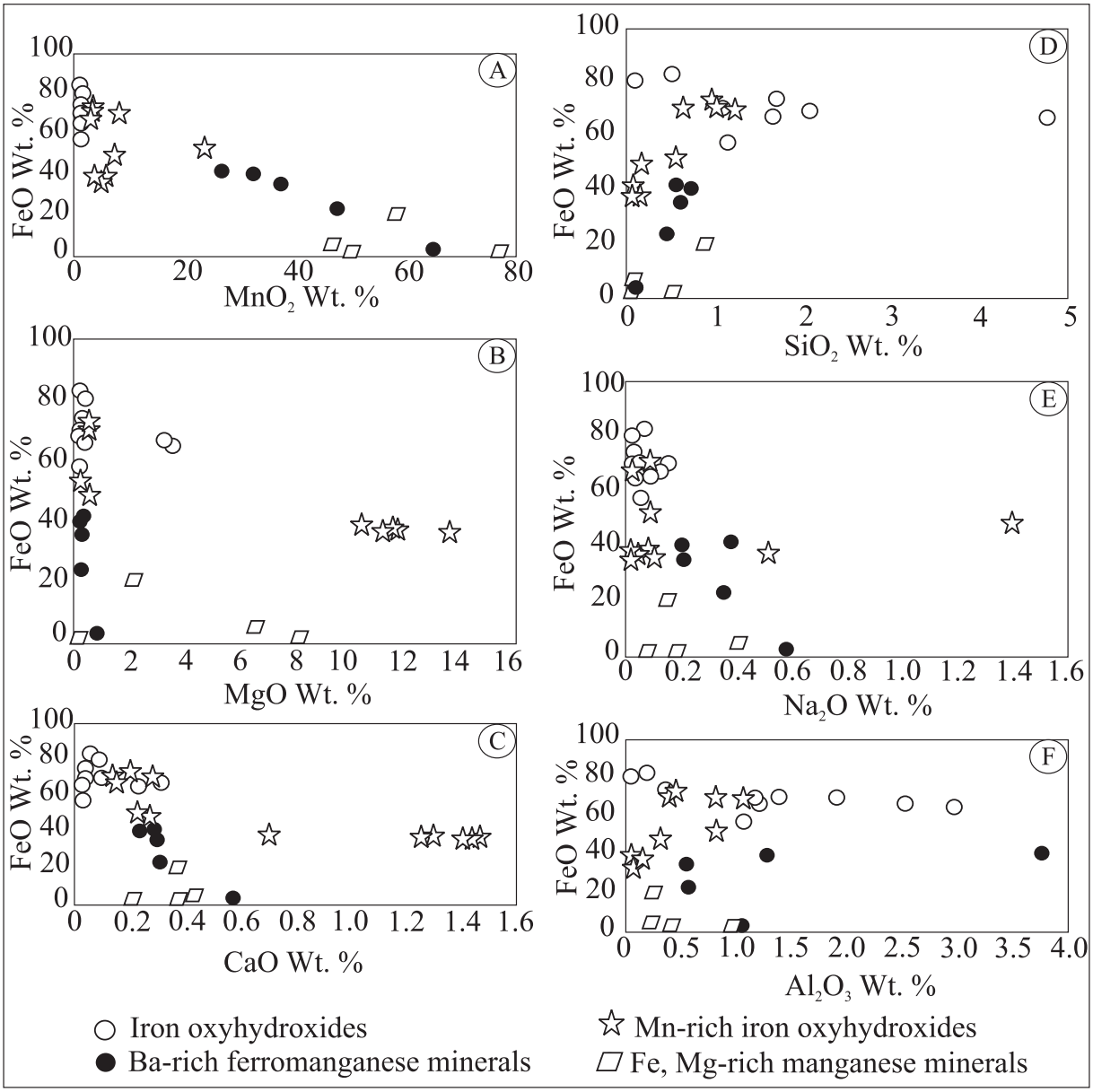

Fig. 8. Correlation between the major oxides (FeO vs. MnO_2 (A), MgO (B), CaO (C), SiO_2 (D), Na_2O (E), and vs. Al_2O_3 (F)) in the determined ferromanganese minerals present in the studied Eocene ironstones; values were determined by using electron microprobe analysis.

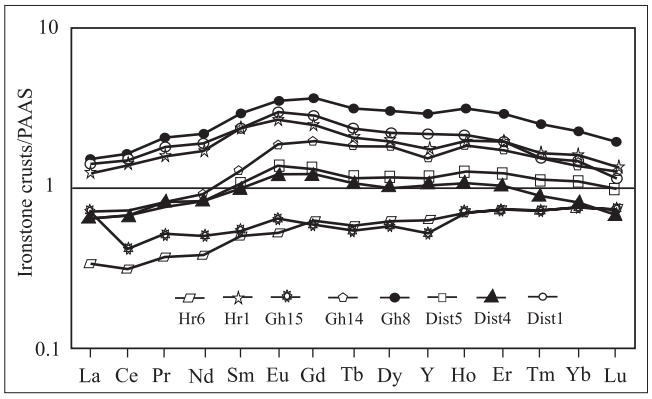

Fig. 9. PAAS-normalized (McLennan, 1989) REE + Y distribution patterns for the upper Cretaceous ironstones (Gh – Ghorabi area samples, Dist – Gabal El-Dist samples, Hr – El Harra area samples).

of the forming fluids as they are not easily fractionated during sedimentation (McLennan, 1989; Bau et al., 1996, 2014; Hein et al., 2016, and references herein). In addition, Bau et al. (2014) provided diagrams for discriminating different origins of ironstones based on rare earth elements and yttrium contents (Fig. 11).

The total REE contents of the upper Cretaceous ironstones (69.61–348.84 ppm) and Eocene ironstones (1.96–89.45 ppm) (Appendices A, B) fall within the range of the ferromanganese deposits of diagenetic origin (110–489 ppm) and hydrothermal origin (15–149 ppm) reported by Bau et al. (2014) and are significantly lower than those usually measured in marine ironstones, which usually range from 1228 to 2282 ppm. Moreover, the marine ferromanganese oxides typically show positive Ce anomalies, negative Y_{SN} values at higher REY concentrations and higher Nd concentrations (> 100 ppm). Consequently, a seawater (marine) origin for the two ironstone types is ruled out (Fig. 11).

REE concentrations are higher in the upper Cretaceous ironstones than in the Eocene ironstones, this being indicative of some

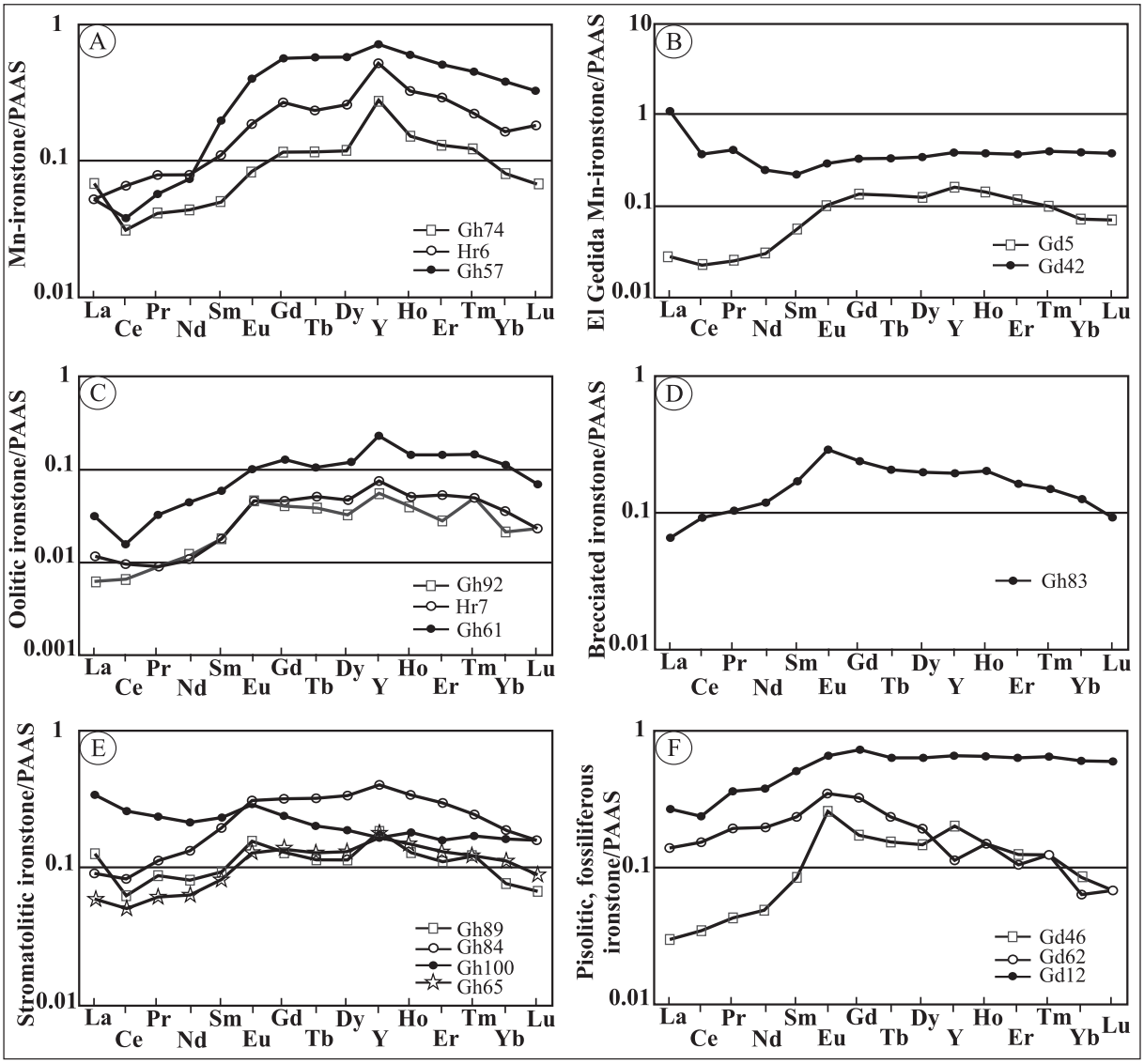

Fig. 10. REE + Y distribution patterns of six types of Eocene ironstones (manganiferous ironstone of Ghorabi and El Harra mines (A), El Gedida manganiferous ironstone (B), oolitic ironstone (C), Brecciated ironstone (D), stromatolitic-like ironstone (E), and pisolitic, fossiliferous ironstone (F)), PAAS-normalized (McLennan, 1989). (Gh – Ghorabi mine samples, Gd – El Gedida mine samples, Hr – El Harra mine samples).

contribution from the associated siliciclastic sediments during their formation. Similar REE + Y values were determined in ferromanganese nodules from the Peru Basin that were interpreted as diagenetic (Von Stackelberg, 1997). These diagenetic Fe–Mn ironstones display negative Y anomalies and negative Ce anomalies, which matches well the results obtained in the ironstone crusts in the Bahariya Depression, i.e. negative Ce anomalies, negative Y anomalies, and intermediate Nd concentrations between 10 and 100 ppm. Accordingly, the REE + Y values support a diagenetic origin for the iron-bearing minerals, thus confirming previous statement by Afify et al. (2015a).

Variations in Ce are controlled by redox reactions and can be clearly observed in the aqueous solutions and their precipitates where cerium has two oxidation states (Bau et al., 1996; Salama et al., 2012 and references therein). The cerium anomaly results from oxidation of Ce^{3+} to Ce^{4+} and subsequent decoupling of Ce from the other REEs due to formation of less soluble Ce^{4+} species and/or preferential adsorption of Ce^{4+} species. In oxidative environments, Ce^{3+} changes to the less soluble Ce^{4+} and thus it removes from the solution, resulting in a negative Ce anomaly relative to its neighbour elements (Bau and Dulski, 1996; Bau et al., 1996; Bolhar et al., 2004). The Ce depletion is evident for the distribution patterns of dissolved rare earth elements under oxic conditions whilst no depletion or even Ce enrichment occurs in anoxic settings. As well, the negative Ce anomalies suggest suboxic conditions wherein aqueous Ce^{3+} is depleted (Kakuwa and Matsumoto, 2006). Thus, the presence of negative Ce anomalies in the two studied ironstone types is attributed to the mixing of iron-rich reducing fluids with oxidized meteoric water.

The used discrimination diagrams also support diagenetic and hydrothermal origin for the upper Cretaceous and Eocene ironstones, respectively (Fig. 11). The diagenetic ironstones show negative Y and Ce anomalies and intermediate Nd concentrations, between 10 and 100 ppm (Bau et al., 2014; Hein et al., 2016). The upper Cretaceous ironstones do not show large positive Ce or any significant Y anomalies, which point to a diagenetic origin from anoxic pore water that moved to the oxidized surface. This result is consistent with the model proposed by Afify et al. (2015a) for these crusts after selective replacement of carbonate minerals during the Turonian-Santonian uplift of the Bahariya area. The geochemical results, mainly Ce and Y obtained from the upper Cretaceous ironstones provide evidence for basinal flow systems associated with hydrocarbons even though they are not preserved. The release of iron by migration of reducing fluids is being increasingly recognized as an effective mechanism in geologic record

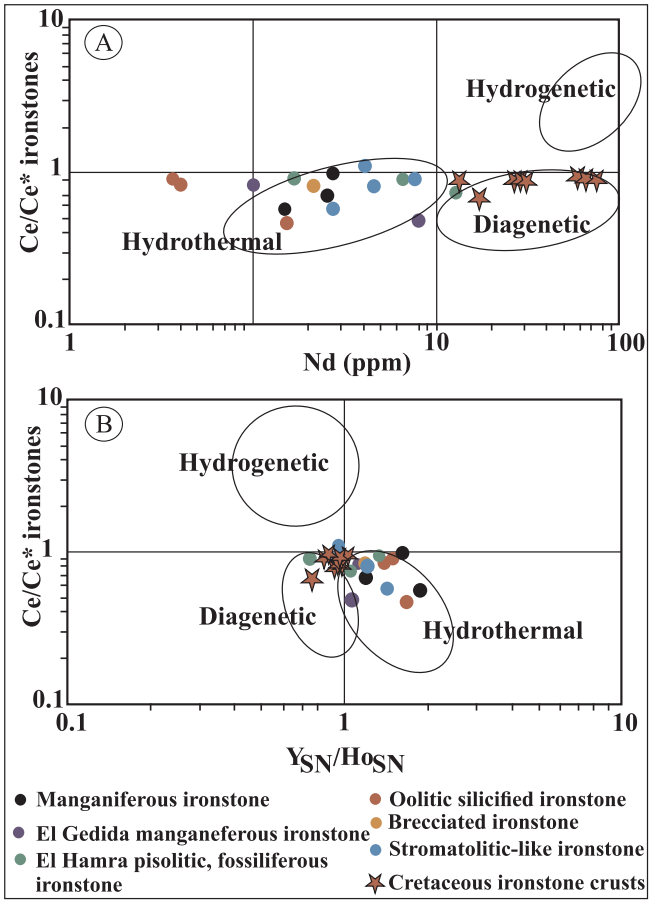

Fig. 11. A. Graph of Ce/Ce* vs. Nd concentration for the different studied ironstones in Bahariya area. B. Binary graph of Ce anomaly vs. Y_{SN}/Ho_{SN} values for the different studied ironstone types (SN: shale normalized). ($Ce/Ce^* = 2Ce_{SN}/(La_{SN} + Pr_{SN})$). The encircled areas in the graph are from Bau et al. (2014).

(Rainoldi et al., 2014, and references therein). On the other hand, the negative Ce anomaly, positive Y and Eu anomalies and the low Nd concentrations together with low concentrations of REE in the Eocene ironstones suggest a hydrothermal origin for this rock type. These results are consistent with the model proposed by Afify et al. (2015b,c) for the Eocene ironstones, which was mainly based on field and petrographic observations. The presence of positive Y anomalies in the Eocene ironstones suggests that precipitation of Fe-Mn minerals occurred very rapidly and immediately after reducing, slightly acidic waters reached more oxidizing and more alkaline water (Bau and Dulski, 1996).

The small positive Eu anomaly in the Eocene ironstones could be a signature inherited from hydrothermal solutions that lost their positive Eu anomaly because of a relatively high oxygen level. This is supported by the fact that, in present oceans, high-temperature hydrothermal solutions lose their Eu anomaly within a few hundred meters away from vent sites due to the rapid oxidation of Eu as a consequence of mixing with oxidized seawater (Klinkhammer et al., 1983). The higher Eu anomaly in the Eocene ironstones than in the Cretaceous ones provides evidence that significantly more REE + Y input from hydrothermal solutions was involved in the formation of the former deposits.

The major faults cutting through the Cenomanian Bahariya Formation and the Eocene carbonate rock units act as a conduit for the hydrothermal solutions during the upper Eocene. The Bahariya Formation was affected by such hydrothermalism around Ghorabi and El Harra mine areas, where the vertical evolution of clay mineral assemblages and transformation of smectite to illite/smectite mixed layer in the Bahariya Formation was present to its upper part (Afify et al., 2014). It was interpreted as a result of increasing temperature affecting the top part of this rock unit where the upper Eocene iron ore deposits occur. This evolution in clay mineralogy was absent in the Cenomanian rocks of Gabal El-Dist where the capping Eocene beds of the Naqb Formation are not replaced by iron (Afify et al., 2014). Nonetheless, this hydrothermalism was not recorded in the REE + Y data of the associated ironstone crusts of the Bahariya Formation.

6. Conclusions

The studied ironstone types show two different models of iron accumulation in siliciclastic and carbonate rocks under contrasted geotectonic conditions. The upper Cretaceous ironstones are diagenetic in origin whilst the ironstones hosted in the Eocene formations formed after Fe, Mn, Si, Ba-rich hydrothermal fluids. The ironstones present in the Cenomanian siliciclastic rocks of the Bahariya Formation formed during telogenetic stages after partial or total dissolution of the carbonate, and concomitant with iron oxyhydroxide formation by mixing of the Fe-rich solutions with meteoric oxygenated water. This was favored by tectonic uplift in the region during the Turonian–Santonian. The iron-bearing minerals from the Bahariya Formation and the underlying Jurassic formations were the source of iron after organic matter decomposition and hydrocarbon migration. In contrast, source of iron for the ironstones hosted in Eocene carbonate rocks was related to deep-seated iron-rich solutions that moved through major faults.

The two ironstone types show some similarities in major and trace element contents, which provide evidence for their formation after carbonate replacement. However, rare earth elements and yttrium (REE + Y) values point to different genetic ironstone types. The Upper Cretaceous ironstones display negative Y and Ce anomalies and intermediate Nd concentrations (between 10 and 100 ppm) indicative of diagenetic origin, whilst the negative Ce anomaly, positive Y and Eu anomalies, low Nd concentration (mostly less than 10 ppm) and very low REE concentrations of the Eocene ironstones strongly support a hydrothermal origin. The presence of positive Y anomalies in the Eocene ironstones suggests that iron precipitation occurred rapidly and immediately after reducing, slightly acidic waters reached oxidizing and alkaline water.

Accordingly, the rare earth elements and yttrium (REE + Y) are good proxies for discriminating the origin of ferromanganese minerals, even in the case that two different types occur in the same stratigraphic succession, as observed in the Bahariya Depression.

Acknowledgments

The authors are grateful to the financial support by the Egyptian Government in a full fellowship during the study of the first author at Complutense University of Madrid, Spain. This work is a part of the activities of Research Groups BSHC UCM-910404 and BSHC UCM-910607. All our gratitude is devoted to Dr. Laura Gonzalez Acebron, Maria Belen Muñoz-Garcia and Valle Lopez (Stratigraphy Department, Faculty of Geological Sciences, UCM), for their great help during the research work. Many thanks to Dr. Cecilia Pérez-Soba Aguilar (Petrology and Geochemistry Department, Faculty of Geological Sciences, UCM), for her help and comments on the geochemical studies. A standing ovation, in no particular order, goes to Xabier Arroyo Rey, Isabel Gómez Pinilla, Teresa Benito Criado, Iván Serrano Muñoz, Pedro Lozano and Marián Barajas (Faculty of Geology, UCM) for their help in laboratory studies and mineralogical and geochemical analyses. The authors are indebted to Franco Pirajno (Editor-In-Chief of Ore Geology Reviews) and İlkay Kuscu (Associate Editor of Ore Geology Reviews) for reviewing and editing of the manuscript. We are so grateful to the reviewers Dr. Walid S. Salama (CSIRO, Western Australia) and the anonymous reviewer for their encouraging comments and annotations that greatly improved an earlier version of the manuscript.

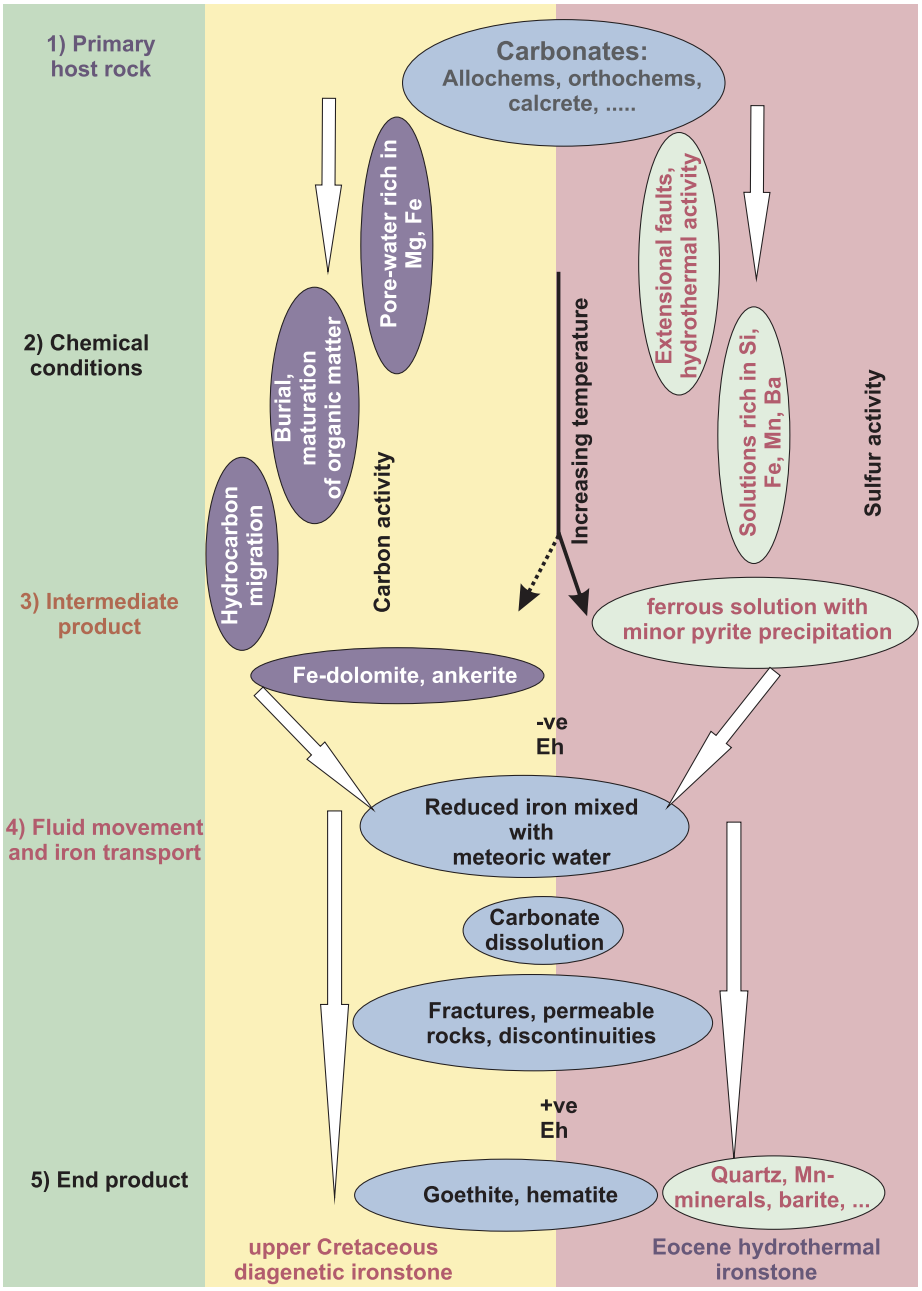

Fig. 12. Sketch showing comparison between the two different models of ironstone formations: upper Cretaceous diagenetic ironstones and Eocene hydrothermal ironstones, studied in the Bahariya Depression.

Appendix A. Supplementary data

Supplementary data associated with this article can be found, in the online version, at http://dx.doi.org/10.1016/j.oregeorev.2018.04.019.

References

Afify, A.M., 2016. Ironstone occurrences in the northern part of the Bahariya Depression, Western Desert, Egypt: Geology, mineralogy, geochemistry and origin. PhD thesis, Universidad Complutense de Madrid, Spain.

Afify, A.M., Arroyo, X., Sanz-Montero, M.E., Calvo, J.P., 2014. Clay mineralogy in Bahariya area, Egypt: Hydrothermal implications on fault-related iron ore deposits, In: 7th Mid European Clay Conference, Germany, Abstract, pp. 137.

Afify, A.M., Sanz-Montero, M.E., Calvo, J.P., Wanas, H.A., 2015a. Diagenetic origin of ironstone crusts in the Lower Cenomanian Bahariya Formation, Bahariya Depression, Western Desert Egypt. J. Afr. Earth Sci. 101, 333–349.

Afify, A.M., Sanz-Montero, M.E., Calvo, J.P., 2015b. Ironstone deposits hosted in Eocene carbonates from Bahariya (Egypt) – New perspective on cherty ironstone occurrences. Sediment. Geol. 329, 81–97.

Afify, A.M., Serra-Kiel, J., Sanz-Montero, M.E., Calvo, J.P., Sallam, E.S., 2016. Nummulite biostratigraphy of the Eocene succession in the Bahariya Depression, Egypt: Implications for timing of iron mineralization. J. Afr. Earth Sci. 120, 44–55.

Baioumy, H.M., Ahmed, H.H., Mohamed, Z.K., 2014. A mixed hydrogeneous and hydrothermal origin of the Bahariya iron ores, Egypt: evidences from the trace and rare earth elements geochemistry. J. Geochem. Expl. 146, 149–162.

Baioumy, H.M., Khedr, M.Z., Ahmed, A.H., 2013. Mineralogy, geochemistry and origin of Mn in the high-Mn iron ores, Bahariya Oasis Egypt. Ore Geol. Rev. 53, 63–76.

Basta, E.Z., Amer, H.I., 1969. El Gedida iron ores and their origin, Bahariya oasis, Western Desert, U.A.R. Econ. Geol. 64, 424–444.

Bau, M., 1996. Controls on the fractionation of isovalent trace elements in magmatic and aqueous systems: evidence from Y/Ho, Zr/Hf, and lanthanide tetrad effect. Contrib. Mineral. Petrol. 123, 323–333.

Bau, M., Dulski, P., 1996. Distribution of yttrium and rare-earth elements in the Penge and Kuruman iron-formations, Transvaal Supergroup, South Africa. Precambr. Res. 79, 37–55.

Bau, M., Dulski, P., 1999. Comparing yttrium and rare earths in hydrothermal fluids from the Mid-Atlantic Ridge: implications for Y and REE behavior during near-vent mixing and for the Y/Ho ratio of Proterozoic seawater. Chem. Geol. 155, 77–90.

Bau, M., Koschinsky, A., Dulski, P., Hein, J.R., 1996. Comparison of the partitioning

behaviours of yttrium, rare earth elements, and titanium between hydrogenetic marine ferromanganese crusts and seawater. Geochim. Cosmochim. Acta 60, 1709–1725.
Bau, M., Möller, P., 1992. Rare earth element fractionation in metamorphogenic hydrothermal calcite, magnesite and siderite. Mineral. Petrol. 45, 231–246.
Bau, M., Schmidt, K., Koschinsky, A., Hein, J., Kuhn, T., Usui, A., 2014. Discriminating between different genetic types of marine ferro-manganese crusts and nodules based on rare earth elements and yttrium. Chem. Geol. 381, 1–9.
Bekker, A., Planavsky, N.J., Krapež, B., Rasmussen, B., Hofmann, A., Slack, J.F., Rouxel, O.J., Konhauser, K.O., 2014. Iron formations: their origins and implications for ancient seawater chemistry. Treat. Geochem. (Second Edition) 9, 561–628.
Bekker, A., Slack, J.F., Planavsky, N., et al., 2010. Iron formation: the sedimentary product of the complex interplay among mantle, tectonic, oceanic, and biospheric processes. Econ. Geol. 105, 467–508.
Bhattacharyya, D.P., Kakimoto, P., 1982. Origin of ferriferous ooids: an SEM study of ironstone ooids and bauxite pisoids. J. Sediment. Petrol. 52, 849–857.
Bolhar, R., Kamber, B.S., Moorbath, S., Fedo, C.M., Whitehouse, M.J., 2004. Characterization of Early Archaean chemical sediments by trace element signatures. Earth Planet. Sci. Lett. 222, 43–60.
Catuneanu, O., Khalifa, M.A., Wanas, H.A., 2006. Sequence stratigraphy of the Lower Cenomanian Bahariya Formation, Bahariya Oasis, Western Desert Egypt. Sediment. Geol. 190, 121–137.
Chan, M.A., Parry, W.T., Bowman, J.R., 2000. Diagenetic hematite and manganese oxides and fault-related fluid flow in Jurassic sandstones, southeastern Utah. Am. Assoc. Petrol. Geol. Bull. 84, 1281–1310.
Chen, D., Qing, H., Yan, X., Li, H., 2006. Hydrothermal venting and basin evolution (Devonian, South China): constraints from rare earth element geochemistry of chert. Sediment. Geol. 183, 203–216.
Dabous, A.A., 2002. Uranium isotopic evidence for the origin of the Bahariya iron deposits Egypt. Ore Geol. Rev. 19, 165–186.
Deer, W.A., Howie, R.A., Zussman, J., 1992. An Introduction to the Rockforming Minerals (second ed.). Essex Longman Scientific and Technical, New York Wiley pp. 696.
El Akkad, S.E., Issawi, B., 1963. Geology and iron ore deposits of Bahariya Oasis. Geol. Surv. Egypt 18, 300.
El Aref, M.M., Lotfy, Z.H., 1985. Genetic karst significance of the iron ore deposits of El Bahariya Oasis, Western Desert. Ann. Geol. Surv. Egypt 15, 1–30.
El Aref, M.M., El Sharkawi, M.A., Khalil, M.A., 1999. Geology and genesis of the strata-bound and Stratiform Cretaceous–Eocene iron ore deposits of the Bahariya region, Western Desert, Egypt. GAW 4th International Conference, Cairo University, Egypt, pp. 450–475.
El Aref, M.M., Mesaed, A.A., Khalil, M.A., Salama, W.S., 2006a. Stratigraphic setting, facies analyses and depositional environments of the Eocene ironstones of Gabal Ghorabi mine area, El Bahariya Depression, Western Desert Egypt. Egypt. J. Geol. 50, 29–57.
El Aref, M.M., Mesaed, A.A., Khalil, M.A., Salama, W.S., 2006b. Microbialite morphostructures and biogenic accretion mechanism of the Eocene ironstones of Gabal Ghorabi mine area, El Bahariya Depression, Western Desert Egypt. Egypt. J. Geol. 50, 59–81.
El-Etr, H.A., Moustafa, A.R., 1978. Field relations of the main basalt occurrences of the Bahariya Region, central Western Desert Egypt. Proceed. Egypt. Acad. Sci. 31, 191–201.
El Sharkawi, M.A., Higazi, M.M., Khalil, N.A., 1984. Three genetic iron ore dikes of iron ores at El Gedida mine, Western Desert, Egypt Geological Society of Egypt. in: 21st Annual Meeting, Cairo, Egypt, pp. 68.
Harder, H., 1989. Mineral genesis in ironstones: a model based upon laboratory experiments and petrographic observations. In: Young, T.P., Taylor, W.E.G. (Eds.), Phanerozoic Ironstones. Geological Society of London, Special Publication pp. 9–18.
Hein, J.R., Conrad, T., Mizell, K., Banakar, K.V., Frey, F.A., Sager, W.W., 2016. Controls on ferromanganese crust composition and reconnaissance resource potential, Ninetyeast Ridge, Indian Ocean. Deep-Sea Res. I 110, 1–19.
Hein, J.R., Koschinsky, A., Halbach, P., Manheim, F.T., Bau, M., Kang, J.-K., Lubick, N., 1997. Iron and manganese oxide mineralization in the Pacific. In: Nicholson, K. (Ed.), Manganese Mineralization: Geochemistry and Mineralogy of Terrestrial and Marine Deposits. Geological Society, Special Publication pp. 123–138.
Hein, J.R., Schulz, M.S., Dunham, R.E., Stern, R.J., Bloomer, S.H., 2008. Diffuse flow hydrothermal manganese mineralization along the active Mariana and southern Izu-Bonin arc system, western Pacific. J. Geophys. Res. 113, 1–29.
Heikoop, J.M., Tsujita, C.J., Risk, M.J., Tomascik, T., Mah, A.J., 1996. Modern iron ooids from a shallow-marine volcanic setting: Mahengetang, Indonesia. Geology 24, 759–762.
Helba, A.A., El Aref, M.M., Saad, F., 2001. Lutetian oncoidal and ooidal ironstone sequence; depositional setting and origin; northeast El Bahariya Depression, Western Desert Egypt. Egypt. J. Geol. 45 (1A), 325–351.
James, H.L., 1966, Chemistry of Iron-Rich Sedimentary Rocks: Data of Geochemistry, 6th ed.: US Geological Survey Professional Paper 440-W.
Jochum, K.P., Seufert, H.M., Spettel, B., 1986. The solar-system abundances of Nb, Ta, Y, and the relative abundances of refractory lithophile elements in differentiated planetary bodies. Geochim. Cosmochim. Acta 50, 1173–1183.
Kakuwa, Y., Matsumoto, R., 2006. Cerium negative anomaly just before the Permian and Triassic boundary event–The upward expansion of anoxia in the water column. Palaeogeogr. Palaeoclimatol. Palaeoecol. 229, 335–344.
Kappler, A., Pasquero, C., Konhauser, K.O., Newman, D.K., 2005. Deposition of banded iron formations by anoxygenic phototropic Fe(II)-oxidizing bacteria. Geology 33, 865–868.
Kimberley, M.M., 1979. Origin of oolitic iron formations. J. Sediment. Petrol. 49, 111–132.
Kimberley, M.M., 1989. Exhalative origins of iron formations. Ore Geol. Rev. 5, 13–145.
Kimberley, M.M., 1994. Debate about ironstone: has solute supply been surficial weathering, hydrothermal convection, or exhalation of deep fluids? Terra Nova 6, 116–132.
Klinkhammer, G., Elderfield, H., Hudson, A., 1983. Rare earth elements in seawater near hydrothermal vents. Nature 305, 185–188.
Loope, D.B., Kettler, R.M., Webber, K.A., 2011. Morphologic clues to the origins of iron oxide–cemented spheroids, boxworks, and pipelike concretions, Navajo Sandstone of South-Central Utah, U.S.A. J. Geol. 119, 505–520.
McLennan, S.M., 1989. Rare earth elements in sedimentary rocks: Influence of provenance and sedimentary processes. In: Lipin, B.R., McKay, G.A. (Eds.), Geochemistry and Mineralogy of Rare Earth Elements. Reviews in Mineralogy and Geochemistry. Mineralogical Society of America, Washington, D.C. pp. 169–200.
Meneisy, M.Y., 1990. Vulcanicity. In: Said, R. (Ed.), The Geology of Egypt. A.A Balkema, Rotterdam, pp. 57–172.
Mesaed, A.A., 2006. Mechanism of formation of the Cenomanian glauconitic ironstones of the Bahariya Formation, Gabal el Dist, Bahariya Oases, Western Desert, Egypt. Bull. Teth. Geol. Soc. Cairo 1, 17–36.
Metwalli, F.I., Pigott, J.D., 2005. Analysis of petroleum system criticals of the Matruh-Shushan Basin, Western Desert. Egypt. Petrol. Geosci. 11, 157–178.
Moustafa, A.R., Saoudi, A., Moubasher, A., Ibrahim, I.M., Molokhia, H., Schwartz, B., 2003. Structural setting and tectonic evolution of the Bahariya Depression, Western Desert, Egypt. GeoArabia, 8. Gulf Petrolink, Bahrain, pp. 91–124.
Mücke, A., 2000. Environmental conditions in the late Cretaceous African Tethys: conclusions from a microscopic-michrochemical study of ooidal ironstones from Egypt, Sudan and Nigeria. J. Afr. Earth Sci. 30, 25–46.
Mücke, A., Agthe, Ch., 1988. Mineralization, origin and age classification of ferruginized sandstone in the Bahariya Oasis, Western Desert, Egypt: a contribution to the origin of red beds. Lithos 22 (1), 59–73.
Mücke, A., Farshad, F., 2005. Whole-rock and mineralogical composition of Phanerozoic ooidal ironstones: comparison and differentiation of types and subtypes. Ore Geol. Rev. 26, 227–262.
Nicholson, K., 1992. Contrasting mineralogical – geochemical signatures of manganese oxides: guides to metallogenesis. Econ. Geol. 87, 1253–1264.
Odah, H., 2004. Paleomagnetism of the Upper Cretaceous Bahariya Formation, Bahariya Oasis, Western Desert, Egypt. J. Appl. Geophys. 3 (2), 177–187.
Owen, A.W., Armstrong, H.A., Floyd, J.D., 1999. Rare earth elements in chert clasts as provenance indicators in the Ordovician and Silurian of the Southern Uplands of Scotland. Sediment. Geol. 124, 185–195.
Parry, W.T., 2011. Composition, nucleation, and growth of iron oxide concretions in the Jurassic Navajo Sandstone, Utah. Sediment. Geol. 233, 53–68.
Parry, W.T., Chan, M.A., Nash, B.P., 2009. Diagenetic characteristics of the Jurassic Navajo Sandstone in the Covenant oil fi eld, central Utah thrust belt. Am. Assoc. Petrol. Geol. Bull. 93, 1039–1061.
Rainoldi, A.L., Franchini, M., Beaufort, D., Patrier, P., Giusiano, A., Impiccini, A., Pons, J., 2014. Large-scale bleaching of red beds related to upward migration of hydrocarbons: Los Chihuidos High, Neuquén basin, Argentina. J. Sediment. Res. 84, 373–393.
Rasmussen, B., Krapez, B., Meier, D.B., 2014. Replacement origin for hematite in 2.5 Ga banded iron formation: evidence for postdepositional oxidation of iron-bearing minerals. Geol. Soc. Am. Bull. 126, 438–446.
Rivas-Sánchez, M.L., Alva-Valdivia, L.M., Arenas-Alatorre, J., Urrutiafucugauchi, J., Ruiz-Sandoval, M., Ramos-Molina, M.A., 2006. Berthierine and chamosite hydrothermal: Genetic guides in the Peña Colorada magnetite-bearing ore deposit, Mexico: earth. Planet. Space 58, 1389–1400.
Rossi, C., Goldstein, R.H., Ceriani, A., Marfil, R., 2002. Fluid inclusions record thermal and fluid evolution in reservoir sandstones, Khatatba Formation, Western Desert, Egypt: a case for fluid injection. Am. Assoc. Petrol. Geol. (AAPG) Bull. 86, 1773–1799.
Rossi, C., Marfil, R., Ramseyer, K., Permanyer, A., 2001. Facies-related diagenesis and multiphase siderite cementation and dissolution in the reservoir sandstones of the Khatatba Formation, Egypt's Western Desert. J. Sediment. Res. 71, 459–472.
Said, R., Issawi, B., 1964. Geology of the northern plateau, Bahariya Oasis, Egypt. Geol. Surv. Egypt 29, 41.
Salama, W., El Aref, M.M., Gaupp, R., 2012. Mineralogical and geochemical investigations of the Middle Eocene ironstones, El Bahariya Depression, Western Desert, Egypt. Gondw. Res. 22, 717–736.
Salama, W., El Aref, M.M., Gaupp, R., 2013. Mineral evolution and processes of ferruginous microbialite accretion – an example from the Middle Eocene stromatolitic and ooidal ironstones of the Bahariya Depression, Western Desert, Egypt. Geobiology 11, 15–28.
Salama, W., El Aref, M.M., Gaupp, R., 2014. Facies analysis and palaeoclimatic significance of ironstones formed during the Eocene greenhouse. Sedimentology 61, 1594–1624.
Salama, W., El Aref, M.M., Gaupp, R., 2015. Spectroscopic characterization of iron ores formed in different geological environments using FTIR, XPS, Mössbauer spectroscopy and thermoanalyses. Spectrochim. Acta Part A Mol. Biomol. Spectrosc. 136, 1816–1826.
Sehim, A.A., 1993. Cretaceous tectonics in Egypt. Egypt. J. Geol. 37, 335–372.
Siehl, A., Thein, J., 1989. Minette-type ironstones. In: Young, T.P., Taylor, W.E.G. (Eds.), Phanerozoic Ironstones. Geological Society of London, Special Publication, pp. 175–193.
Stanton, R.L., 1972. Ore Petrology. McGraw-Hill pp. 771.
Sturesson, U., Dronov, A., Saadre, T., 1999. Lower Ordovician iron ooids and associated oolitic clays in Russia and Estonia. Sediment. Geol. 123, 63–80.
Sturesson, U., Keikoop, J.M., Risk, M.J., 2000. Modern and Paleozoic iron ooids – a similar volcanic origin. Sediment. Geol. 136, 137–146.
Sun, S., Konhauser, K.O., Kappler, A., Li, Y.L., 2015. Primary hematite in Neoarchean to

Paleoproterozoic oceans. Geol. Soc. Am. Bull. 127, 850–861.
Tanner, L.H., Khalifa, M.A., 2010. Origin of ferricretes in fluvial-marine deposits of the Lower Cenomanian Bahariya Formation, Bahariya Oasis, Western Desert, Egypt. J. Afr. Earth Sci. 56, 179–189.
Taylor, S.R., McLennan, S.M., 1985. The Continental Crust: Its Composition and Evolution. Blackwell, Oxford.
Van Houten, F.B., Purucker, M.E., 1984. Glauconitic peloids and chamositic ooids – favourable factors, constraints and problems. Earth Sci. Rev. 20, 211–243.
Von Stackelberg, U., 1997. Growth history of manganese nodules and crust of the Peru Basin. In: Nicholson, K., Hein, J.R., Buhn, B., Dasgupta, S. (Eds.), Manganese Mineralization: Geochemistry and Mineralogy of Terrestrial and Marine Deposits. Geological Society of London, Special Publication, pp. 153–176.
Young, T.P., Taylor, W.G.E., 1989. Phanerozoic ironstones. Geological Society London Special Publication pp. 251.